Coordination of Cu(II) to Lipophilic Bis-hydroxamate Binders As Studied by One- and Two-Dimensional Electron Spin Echo Spectroscopy

V. Kofman,[†] J. J. Shane,[†] S. A. Dikanov,[‡,§] M. K. Bowman,[§] J. Libman,[⊥] A. Shanzer,[⊥] and D. Goldfarb*,[†]

Contribution from the Departments of Chemical Physics and Organic Chemistry, Weizmann Institute of Science, 76100 Rehovot, Israel, Institute of Chemical Kinetics and Combustion, Novosibirsk, 630090, Russian Federation, and Macromolecular Structure and Dynamics, Environmental Molecular Science Laboratory, Pacific Northwest Laboratories, Richland, Washington 99352

Received June 19, 1995[⊗]

Abstract: The binding of Cu(II) to a lipophilic bis-hydroxamate binder, RL252, and its parent RL239, was investigated by pulsed EPR. The binders have two arms, each terminated with a hydroxamate group which serves as a donor. The major difference between RL252 and RL239 is the absence of the leucine amino acid bridge in RL239. Orientation-selective electron spin echo envelope modulation (ESEEM) experiments were carried out at 8.45 and 9.15 GHz. The spectra obtained were exceptionally well resolved and indicated that the cancellation condition, which requires that the hyperfine coupling is approximately twice the nuclear Larmor frequency, is met at 8−9 GHz. The spectra of both Cu−RL252 and Cu−RL239 showed the nuclear quadrupole resonance (NQR) frequencies, ν_0, ν_-, and ν_+, of the ^{14}N of the hydroxamate groups at 1.6−1.7, 2.15−2.25, and 3.8−3.9 MHz. A peak corresponding to the double quantum transition in the "noncanceled manifold", ν_{DQ}, was observed at 5−5.2 MHz, and at some magnetic fields a peak corresponding to a single quantum transition, ν_{SQ}, and its combination harmonic appeared as well. The assignment of all the ESEEM frequencies was achieved by the application of the two-dimensional hyperfine sublevel correlation (HYSCORE) experiment. Following the assignment, simulations of the orientation-selective ESEEM spectra were performed, yielding the magnitude and orientation of the quadrupole and hyperfine tensors of the coupled nitrogens. While only one best fit set of quadrupolar parameters was found, two such sets were obtained for the hyperfine interaction. Analysis of the orientation of the quadrupole tensor with respect to the g-tensor showed that in both Cu−RL252 and Cu−RL239 the binding site is close to coplanar. Very subtle differences in the spin Hamiltonian parameters were observed between Cu−RL252 and Cu−RL239. The ^{14}N quadrupolar parameters and the anisotropic hyperfine component were slightly larger in Cu−RL239. The relatively small ^{14}N hyperfine coupling is attributed to a node in the molecular orbital, occupied by the unpaired electron, at the nitrogen.

Introduction

Lipophilic carriers of metal ions are of great interest for biological applications in view of their capability to penetrate biological membranes. Thanks to these properties, such compounds may function either as scavengers of intracellular metal ions, or as carriers for the delivery of metal ions needed in the cell. One example is the use of lipophilic ion carriers for the removal of iron from red blood cells.[1−3] Such carriers have been shown to provide potential antimalarial agents by inhibiting intracellular parasite growth. Another example is the use of lipophilic bis-hydroxamate carriers for the delivery of vanadyl ions to fat cells.[4] Vanadyl ions have been shown to simulate most of the properties of insulin, and their effective intracellular delivery has been demonstrated to significantly augment their insulinomimetic properties. Recently, a lipophilic bis-hydroxamate for Cu(II) (termed RL252, Figure 1) was designed and synthesized. The Cu(II) replaces the two protons, thus forming a neutral complex. It is a highly selective Cu(II)-extractant, and it selectively transports Cu(II) across artificial membranes in the presence of five competing metal ions, namely Co(II), Ni(II), Zn(II), Cd(II), and Pb(II).[5] RL252 proved to bind Cu(II) with an exceptionally high binding constant, $\log \beta_2 = 13.95$[6] and thereby to significantly exceed the binding efficiency of a single acetohydroxamate moiety.[7] The unique Cu(II)-binding characteristics of RL252, and the lack of any crystallographic data on Cu(II)−bis-hydroxamates (except for some powder data[8]), prompted us to examine the Cu(II)−bis-hydroxamate configuration of Cu−RL252 as a prototype of Cu(II)−bis-hydroxamate. Encouraged by the recent application of electron spin echo envelope modulation (ESEEM) spectroscopy for the characterization of the vanadyl−bis-hydroxamates,[9] orientation-selective three-pulse ESEEM along with two-dimensional (2D)

[†] Department of Chemical Physics.
[‡] Institute of Chemical Kinetics and Combustion.
[§] Macromolecular Structure and Dynamics.
[⊥] Department of Organic Chemistry.
[⊗] Abstract published in *Advance ACS Abstracts*, December 1, 1995.

(1) Shanzer, A.; Libman, J.; Lytton, S.; Glickstein, Z.; Cabantchik, Z. I. *Proc. Natl. Acad. Sci.* **1991**, *88*, 6585.
(2) Lytton, S. D.; Mester, B.; Dayan, I.; Glickstein, H.; Libman, J.; Shanzer, A.; Cabantchik, Z. I. *Blood* **1993**, *81*, 214.
(3) Lytton, S. D.; Mester, B.; Landau, I.; Libman, J.; Shanzer, A.; Cabantchik, Z. I. *Am. J. Hematol.* **1993**, *43*, 217.
(4) Shechter, Y.; Shisheva, A.; Lazar, R.; Libman, J.; Shanzer, A. *Biochemistry* **1992**, *31*, 2063.
(5) Bromberg, L.; Levin, G.; Libman, L.; Shanzer, A. *J. Membrane Sci.* **1992**, *69*, 143.
(6) Farkas, E. Unpublished results.
(7) Schwartenbach, G.; Schwartenbach, K. *Helv. Chim. Acta* **1963**, *46*, 1390.
(8) Hutchinson, B.; Bostick, Y.; Crowder, Y.; Eversdyk, D.; Hurley, D.; Jett, D.; Olbricht, S.; Sample, S.; Thompson, L. *Inorg. Chim. Acta* **1983**, *74*, 29.
(9) Kofman, V.; Dikanov, S. A.; Haran, A.; Libman, J.; Shanzer, A.; Goldfarb, D. *J. Am. Chem. Soc.* **1995**, *117*, 383.

0002-7863/95/1517-12771$09.00/0

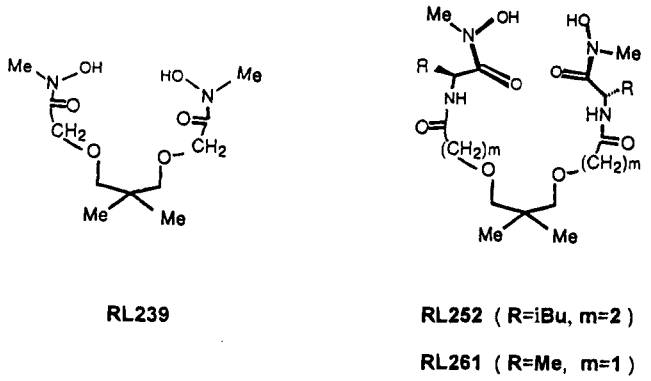

RL239

RL252 (R=iBu, m=2)

RL261 (R=Me, m=1)

Figure 1. Schematic structures of the bis-hydroxamate binders.

hyperfine sublevel correlation (HYSCORE) experiments[10] were applied to study the binding geometry of Cu−RL252 and Cu−RL239 (Figure 1).

The ESEEM method was particularly effective for investigating the structure of the binding site of the VO(II) complexes due to the so-called "exact cancellation condition"[11] which for the hydroxamate nitrogens is met at X-band EPR frequency (~9 GHz).[9] The cancellation condition requires that the hyperfine coupling is approximately twice the Larmor frequency of the nitrogen ($2\nu_N \approx a_{iso}$), leading to an effective field close to zero in one of the electron spin manifolds due to the cancellation of the nuclear Zeeman field by the hyperfine field. The modulation frequencies corresponding to nuclear transitions within this manifold are, therefore, the nuclear quadrupole resonance (NQR) frequencies, ν_o, ν_-, ν_+.[11,12] The Fourier-transformed (FT) ESEEM spectrum of an orientationally disordered system typically consists of the three peaks at the NQR frequencies and a fourth line corresponding to the $\Delta m_I = 2$ transition (ν_{DQ}) in the other electron spin manifold. The other two signals, corresponding to single quantum transitions (ν_{SQ}, $\Delta m_I = 1$) within this manifold, are usually broadened beyond detection.[11] When the EPR spectrum is governed by a large anisotropic interaction it is possible to perform orientation-selective ESEEM experiments[13] which provide the anisotropic component of the hyperfine interaction[14] and the orientation of the hyperfine and quadrupole tensors.[14,15]

As in the VO(II)−bis-hydroxamate complexes,[9] the hyperfine coupling of the hydroxamate nitrogens in the Cu(II) complexes fulfills the cancellation condition at ~9 GHz, hence providing the means to determine their hyperfine and quadrupole interactions and the geometry of the binding site. The orientation-selective FT-ESEEM spectra of the Cu(II) complexes are exceptionally well resolved, and in some spectra ν_{SQ} can be observed. Complete assignment of the spectra was achieved by the application of the 2D HYSCORE experiment which generates spectra with cross peaks between ESEEM frequencies belonging to different M_S manifolds.[10,16] So far, only a few examples of the effectiveness of HYSCORE in peak assignment have been reported[16] and this work demonstrates the advantage of this experiment over the standard ESEEM approaches. The structure of the Cu(II) binding site in Cu−RL252 and Cu−RL239 was found to be close to square coplanar, and only small differences were observed in the spectroscopic properties of Cu−RL252 and Cu−RL239.

Experimental Section

Ligand Synthesis. The hydroxamate ligands were prepared as described previously.[17] The preparation involved essentially three steps: (i) preparation of the bis-pentachlorophenolates $(CH_3)_2(CH_2OCH_2COOC_6Cl_5)_2$, (ii) preparation of the aminohydroxamate $H_2NCHiBuCONOHCH_3$, and (iii) coupling of the phenolates with *N*-hydroxylamine to provide RL239 and with aminohydroxamate to provide RL252. Both compounds were purified by column chromatography and were fully characterized by their spectroscopic features, which were in agreement with the assigned structures.

Sample Preparations. 50 μL of a methanol or acetonitrile solution of the ligand (5 or 10 mM) were mixed with 10 μL of an aqueous solution of $CuSO_4$ (20 mM). The resulting solution was then transferred into an EPR quartz tube (3 mm o.d.) and sealed.

Spectroscopic Measurements. Continuous wave (CW) EPR measurements were performed at 140−150 K on a Varian E-12 spectrometer operating at ~9.3 GHz. The X-band ESEEM and 2D HYSCORE experiments were carried out at 4−10 K at frequencies around 9.3 and 8.5 GHz, using a home built spectrometer, described elsewhere.[14] The magnetic field and spectrometer frequency were measured with a Bruker NMR gaussmeter (ER-035M) and a HP-5350B frequency counter. The ESEEM waveforms were recorded using the three-pulse sequence, $\pi/2-\tau-\pi/2-T-\pi/2-\tau-$echo, where the echo intensity is measured as a function of the time interval T. Measurements were carried out at a repetition rate of 100 Hz and τ-values of 180, 220, and 300 ns. Typically, the $\pi/2$ pulse length was 20 ns and T was incremented in steps of 20 ns. 2D HYSCORE spectra were recorded using the sequence $\pi/2-\tau-\pi/2-t_1-\pi-t_2-\pi/2-\tau-$echo, where the echo is measured as a function of t_1 and t_2.[10] The duration of the $\pi/2$ and π pulses was 15 ns and the amplitude of the π pulse was twice that of the $\pi/2$ pulses. From 100 to 140 points were collected in each dimension, and t_1 and t_2 were incremented in steps of 40 ns from their initial value of 90 ns. The appropriate phase cycles, eliminating unwanted echoes, were employed in all experiments.[18,19]

Data Manipulation. (a) 1D ESEEM. To avoid distortions of the FT-ESEEM spectrum due to spectrometer dead time, which for the three-pulse experiment was typically τ + 40 ns, the missing data points were reconstructed using the linear prediction singular value decomposition (LPSVD) method.[20] Prior to Fourier transformation the background decay was subtracted either by a polynomial or exponential fit or by subtracting the appropriate zero frequency component as obtained from the LPSVD procedure, the data were convoluted with an exponential decay, and zero-filling was performed. All spectra shown are the cosine FT-ESEEM.

(b) 2D ESEEM. The background decay in both t_1 and t_2 dimensions was subtracted using a third-order polynomial fit and after convolution with a cosine roll-off function and zero filling to 256 points in each dimension Fourier transformation was carried out in the two dimensions. The spectra shown are contour plots in the magnitude mode with logarithmic scaling of the contour intervals.

Basic Equations and Simulations Procedure. The spin Hamiltonian for Cu(II) (S = 1/2, I = 3/2) interacting with two ^{14}N, I = 1, nuclei is:

$$\mathcal{H} = \frac{\beta}{h}\vec{H}_o\mathbf{g}\hat{S} + \hat{I}\mathbf{A}(^{63,65}\mathrm{Cu})\hat{S} + \mathcal{H}_N \qquad (1)$$

The last term includes the ^{14}N nuclear interactions, which are small relative to the other interactions and in our case do not generate resolved

(10) Höfer, P.; Grupp, A.; Nebenführ, H.; Mehring, M. *Chem. Phys. Lett.* **1986**, *132*, 279.
(11) Mims, W. B.; Peisach, J. *J. Chem. Phys.* **1978**, *69*, 4921.
(12) Flanagan, H. L.; Singel, D. J. *J. Chem. Phys.* **1987**, *87*, 5606.
(13) Hurst, G. C.; Henderson, T. A.; Kreilick, R. W. *J. Am. Chem. Soc.* **1985**, *107*, 7294.
(14) Goldfarb, D.; Fauth, J.-M.; Tor, Y.; Shanzer, A. *J. Am. Chem. Soc.* **1991**, *113*, 1941.
(15) Flanagan, H. L.; Gerfen, G. L.; Lai, A.; Singel, D. J. *J. Chem. Phys.* **1988**, *88*, 2162.
(16) Shane, J. J.; van der Heijden, P. A. A. W.; Reijerse, E. J.; de Boer, E. *Appl. Magn. Res.* **1994**, *6*, 427. Reijerse, E. J.; Shane, J. J.; de Boer, E.; Höfer, P.; Collison, D. In *Electron Magnetic Resonance of Disordered Systems II*; Yordanov, N. D., Ed.; World Scientific: Singapore, 1991; p 253.
(17) Shanzer, A.; Libman, J.; Lifson, S. US Patent 5.101.066, 1992, and US Patent 5.149.845, 1992.
(18) Fauth, J.-M.; Schweiger, A.; Braunschweiler, L.; Forrer, J.; Ernst, R. R. *J. Magn. Res.* **1986**, *66*, 74.
(19) Gemperle, C.; Aebli, G.; Schweiger, A.; Ernst, R. R. *J. Magn. Res.* **1990**, *88*, 241.
(20) Barkhuijsen, H.; de Beer, R.; Bovee, W. M. M. J.; van Ormondt, D. *J. Magn. Res.* **1985**, *61*, 465.

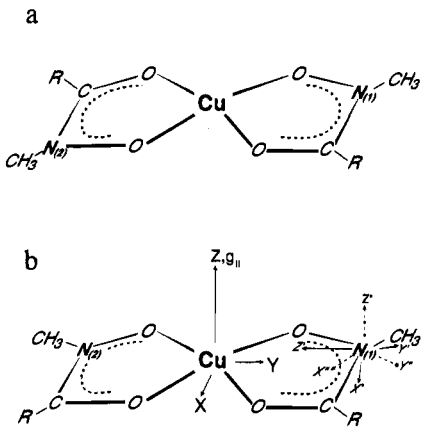

Figure 2. Schematic structures of the Cu(II) binding site and an arbitrary presentation of the coordinate systems. (a) Transoid configuration. (b) Cisoid configuration. The X and Y axes were placed arbitrarily and the same coordination systems applies for both configurations.

splittings in the EPR spectrum. Therefore, simulations of the EPR spectra were done taking into account only the first two terms, treating the hyperfine term by second-order perturbation theory,[21] neglecting the ^{63,65}Cu quadrupole interaction, and assuming that the principal axes of **g** and **A**(^{63,65}Cu) coincide.

The ESEEM waveform can be conveniently calculated using Mims general expressions[22] once the spin Hamiltonian in eq 1 is brought into a block diagonal form, thus defining a nuclear Hamiltonian for each M_S manifold. Diagonalization of the electron Zeeman interaction, neglecting the Cu hyperfine interaction terms,[23] yields the two nuclear Hamiltonians

$$\mathcal{H}_{\alpha,\beta} = \sum_i \left[\frac{g_n \beta_n}{h} \vec{H}_o \hat{I}_i + \hat{I}_i \mathbf{A}'_i \hat{S}'_{\alpha,\beta} + \hat{I}_i \mathbf{Q}_i \hat{I}_i \right] \tag{2}$$

A detailed description of this Hamiltonian is given elsewhere.[14,24,25] The index i denotes the two different nitrogens and $\mathbf{A}'_i = (A_{iso}\mathbf{1} + \mathbf{A}_i)\mathbf{g}$.[14] The principal components of $\mathbf{A}_i$, which is assumed to be axially symmetric and the same for both nitrogens, are $-A_\perp$, $-A_\perp$, and $2A_\perp$. For a small g anisotropy, $a_{iso} \cong A_{iso}g_{iso}$ and $a_\perp \cong A_\perp g_{iso}$. The principal values of the ^{14}N quadrupole tensor, **Q**, are

$$Q^p_{zz} = \frac{e^2qQ}{2h}, \quad Q^p_{xx} = -\frac{1}{2}Q^p_{zz}(1-\eta), \quad \text{and} \quad Q^p_{yy} = -\frac{1}{2}Q^p_{zz}(1+\eta) \tag{3}$$

where η is the asymmetry parameter and $|Q^p_{zz}| \geq |Q^p_{yy}| \geq |Q^p_{xx}|$. The orientation of the external magnetic field, $\vec{H}_o$, with respect to principal axis of **g** (X, Y, Z), is given by θ_o and ϕ_o. The principal axis system of **A**, x', y', z', is transformed into that of **g** using the polar angles θ and ϕ and that of **Q**, x'', y'', z'', by the Euler angles α, β, γ. Figure 2 shows a schematic representation of the binding site and the coordinate systems used. Simulated spectra were generated by numerical diagonalization of the nuclear Hamiltonians described in eq 2, and the eigenvalues and eigenvectors so obtained were used to calculate the modulation patterns using the Mims expressions.[22]

At exact cancellation, ν_o, ν_-, and ν_+, and ν_{DQ} are given by[11,26]

$$\nu_\pm = \frac{3e^2qQ}{4h}\left(1 \pm \frac{\eta}{3}\right), \quad \nu_o = \frac{e^2qQ}{2h}\eta \tag{4}$$

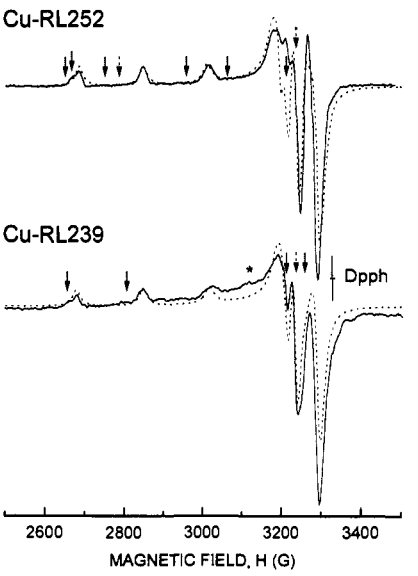

Figure 3. EPR spectra of frozen solutions (150 K) of (top) Cu−RL252 in acetonitrile (9.32 GHz) and (bottom) Cu−RL239 in MeOH (9.32 GHz). The power used was 9 mW, and the modulation amplitude was 6.3 G. The dashed traces represent computer simulations obtained with the parameters given in Table 1. The asterisk denotes spectral features of a minor Cu(II) species. The solid arrows specifies the g-values at which orientation-selective ESEEM experiments were performed and the dotted arrows correspond to positions where HYSCORE was carried out.

$$\nu_{DQ} \cong 2\left[\left(\left|\nu_N\right| + \left|\frac{a_{iso}}{2}\right|\right)^2 + \left(\frac{e^2qQ}{4h}\right)^2(3+\eta^2)\right]^{1/2} \tag{5}$$

where ν_N is the nuclear Larmor frequency. The expression for ν_{DQ} was derived under the assumption that the anisotropic part of the hyperfine interaction can be neglected. Equations 4 and 5 were used to estimate e^2qQ/h, η, and A_{iso} from the experimental positions of the peaks, and the values were then refined by simulations.

The three-pulse echo intensity $E(T,\tau)$ was calculated according to[14,27]

$$E(T,\tau) = \int_{\theta_o}\int_{\phi_o}\frac{1}{2}\left[\prod_i^2 E_i^\alpha(T,\tau) + \prod_i^2 E_i^\beta(T,\tau)\right] f(\theta_o,\phi_o)\sin\theta_o d\theta_o d\phi_o \tag{6}$$

where $f(\theta_o, \phi_o)$ is a weighting function accounting for the inhomogeneous EPR line width and the pulse band width. The ranges of θ_o and ϕ_o that contribute to the echo at each magnetic field within the EPR line shape were determined graphically from plots of the resonant field *vs* θ_o, taking into account the different Cu(M_I) hyperfine components.[14] These were generated by simulations of the EPR spectra in which both the Cu hyperfine and the g-anisotropies were taken into account. For each θ_o a range of 0−180° for ϕ_o was taken. After the zero frequency component was subtracted, the simulated time-domain patterns were convoluted with an exponential decay function with a time-constant of typically 4 μs, to account for relaxation effects, and then Fourier transformation was performed.

Results

The EPR spectra of frozen solutions of Cu−RL252 and Cu−RL239, shown in Figure 3, are similar, and the same spectra were observed for methanol or acetonitrile solutions. While the spectrum of Cu−RL252 is indicative of the existence of only one Cu(II) species the spectrum of Cu−RL239 shows the presence of an additional minor species. Coarse simulations of the EPR spectra were carried out in order to obtain the g and Cu hyperfine matrices from which the orientations con-

(21) Ovchinnikov, I. V.; Konstantinov, V. N. *J. Magn. Res.* **1978**, *32*, 179.
(22) Mims, W. B. *Phys. Rev. B* **1972**, *5*, 2409; **1973**, *6*, 3543.
(23) Gerfen, G. J.; Singel, D. J. *J. Chem. Phys.* **1990**, *93*, 4571.
(24) Rowan, L. G.; Hahn, E. L.; Mims, W. B. *Phys. Rev. A* **1965**, *137*, 61.
(25) Goldfarb, D.; Kevan, L. *J. Chem. Phys.* **1987**, *87*, 6323.
(26) Dikanov, S. A.; Tsvetkov, Yu. D.; Bowman, M. K.; Astashkin, A. V. *Chem. Phys. Lett.* **1982**, *90*, 149.
(27) Dikanov, S. A.; Yudanov, V. F.; Tsvetkov, Yu. D. *J. Magn. Res.* **1979**, *34*, 631.

Table 1. The EPR Parameters of Cu−RL252 and Cu−RL239

	$g_{\|}$	$g_{\perp}$	$A_{\|}$ (10^{-4} cm^{-1})	$A_{\perp}$ (10^{-4} cm^{-1})
Cu−RL252	2.274	2.061	173	21
Cu−RL239	2.272	2.061	179	15

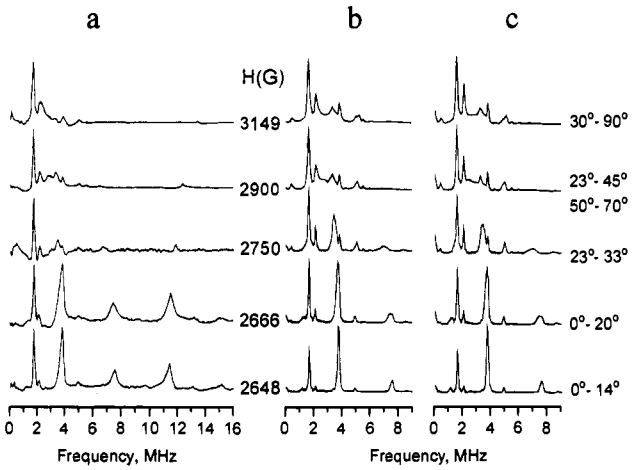

Figure 4. (a) Experimental three-pulse FT-ESEEM spectra of Cu−RL252 in CH_3CN recorded at different magnetic fields within the EPR powder pattern (τ = 0.22 μs, ν = 9.15 GHz, and T = 5 K, for the traces recorded at 2648−2750 G, ν = 9.32 GHz, and for 2900, 3149 G, ν = 9.14 GHz). (b, c) Simulated spectra obtained with parameter sets A and B, respectively, as listed in Table 3 and the same τ values and spectrometer frequency as in (a). The angles listed on the right hand side correspond to the range of θ_o used in the simulations.

tributing to the echo at each magnetic field within the EPR powder pattern were determined. The principal components of these matrices are given in Table 1. These values are typical for tetragonal Cu(II) with four oxygen ligands.[28] The simulations were too coarse to detect any biaxility in **g** or **A**.

Three-pulse FT-ESEEM spectra of Cu−RL252 recorded at 9.13 GHz with τ = 0.22 μs and τ = 0.30 μs at several magnetic fields within the EPR powder pattern (see Figure 3) are presented in Figures 4a and 5a. A signal at the proton Larmor frequency and three peaks at 1.66−1.78, 2.15, and 3.85 MHz are visible in all spectra. These peaks are relatively narrow, and their frequencies are field independent within the range 2648−3150 G. This indicates that at these fields the cancellation condition is met and we thus assign these peaks to the NQR frequencies ν_o, ν_-, and ν_+, respectively. Simulations have shown that the cancellation condition is met when $|\nu_N - (a_{iso}/2)|/\nu_N < 0.25$.[29] Over the range 2648−3150 G, ν_N varies by about 16% which is still within the cancellation range. Low intensity peaks appear at 3.27 MHz in the high field spectra and at ~7.3 MHz in the low field spectra. These are tentatively assigned to the sum combinations of the 1.66 and 3.7 MHz peaks, respectively.

Spectra recorded with τ = 0.22 μs are very similar to those for which τ = 0.3 μs (Figure 5a), the main difference being the reduced intensity of the ν_+ peak for τ = 0.22 μs, due to the suppression effect of τ.[22] For both values of τ, a weak, narrow signal at ~5.1 MHz appears in spectra recorded at magnetic fields within the region of $g_{\perp}$. Orientation-selective three-pulse ESEEM spectra recorded at 8.46 GHz (with τ = 0.22 μs and 0.3 μs) exhibit the same peaks as observed at 9.15 GHz. A slight shift of the 5.1 MHz peak to 5.0 MHz supports its assignment to ν_{DQ}. Similar spectra were obtained for Cu−RL252 in either methanol or acetonitrile solutions.

Usually, the ν_{DQ} peak is broad compared to the NQR peaks and shows a significant field dependence.[14,30] Since this behavior is not observed in our case, the ν_{DQ} peak cannot be assigned on the basis of the 1D ESEEM spectra alone. To unambiguously assign this peak, 2D HYSCORE experiments were carried out. The 2D HYSCORE spectra exhibit cross peaks only between frequencies belonging to different M_S manifolds.[10,16] Therefore, peaks at (ν_{DQ}, ν_o), (ν_{DQ}, ν_-), and (ν_{DQ}, ν_+) are expected. The 2D HYSCORE spectrum of Cu−RL252 in CH_3CN recorded at 3236 G, which corresponds to the resonant magnetic field at which the echo amplitude reaches maximum, is presented in Figure 6b. The spectrum exhibits an intense cross peak at (5.1, 3.8(ν_+)) MHz and a weaker one at (5.1, 2.15(ν_-)) MHz. The appearance of these cross peaks provides an unambiguous assignment of the 5.1 MHz peak to ν_{DQ}. The spectrum also shows a cross peak in the form of a ridge at (2−4, 1.66) MHz attributed to cross peaks between ν_{SQ} and ν_o. A similar spectrum was obtained at H_o = 3256 G and at other τ values.

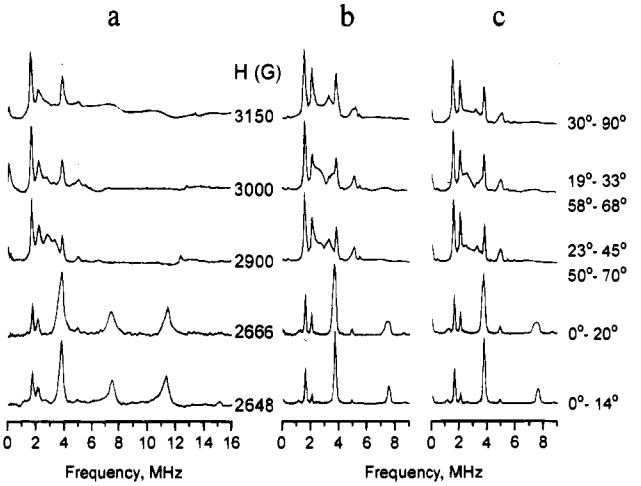

Figure 5. (a) Experimental three-pulse FT-ESEEM spectra of Cu−RL252 in CH_3CN recorded at different magnetic fields within the EPR powder pattern (τ = 0.30 μs, ν = 9.15 MHz, and T = 5 K, for the traces recorded at 2648, 2666 G, ν = 9.32 GHz, for 2900−3150 G, ν = 9.14 GHz). (b, c) Simulated spectra obtained with parameter sets A and B, respectively, as listed in Table 3 and the same τ values and spectrometer frequency as in (a). The angles listed on the right hand side correspond to the range of θ_o used in the simulations.

A 2D HYSCORE spectrum recorded close to the $g_{\|}$ position (2786 G, 9.33 GHz) is shown in Figure 6a. In this spectrum, the cross peak (ν_{SQ}, ν_o) appears as a narrow peak rather than as a ridge, clearly determining the frequency ν_{SQ_1} at 3.6 MHz. The frequency of the second ν_{SQ} can now be determined according to $\nu_{DQ} - \nu_{SQ_1} = \nu_{SQ_2}$, yielding ν_{SQ_2} = 1.4−1.5 MHz. A close look at the 1D spectrum recorded at 2648 G (Figures 4a and 5a) shows a low frequency shoulder at ≈ 1.4 MHz, which can now be attributed to ν_{SQ_2}. The assignment of ν_{SQ_1} indicates that the peak at 3.7−3.8 MHz, observed at low fields in the 1D spectra (Figures 4−5) is a superposition of ν_{SQ_1} and ν_+. The low field 2D HYSCORE spectrum also shows cross peaks at (ν_+, ν_{DQ}) and (ν_o, $2\nu_{SQ}$).

The assignment of the 3.7−3.8 MHz peak observed at low fields to a superposition of ν_{SQ_1} and ν_+ was confirmed by a careful tracking of changes in its width at low fields as shown in Figure 4a. At the lowest field, corresponding to the $g_{\|}$ feature of M_I(Cu) = −3/2, the peak is narrow but as the field increases toward the $g_{\|}$ position of the M_I(Cu) = −1/2 state, where more orientations contribute to the echo, a broadening due to shifts of ν_{SQ_1} is observed. At higher fields, the range of orientations

(28) Peisach, J.; Blumberg, W. E. *Arch. Biochem. Biophys.* **1974**, *185*, 691.

(29) Reijerse, E. J.; Keijzers, C. P. *J. Magn. Reson.* **1987**, *71*, 83.

(30) Jiang, F.; Peisach, J.; Ming, L.-J.; Que, L., Jr.; Chen, V. J. *Biochemistry* **1991**, *30*, 11437.

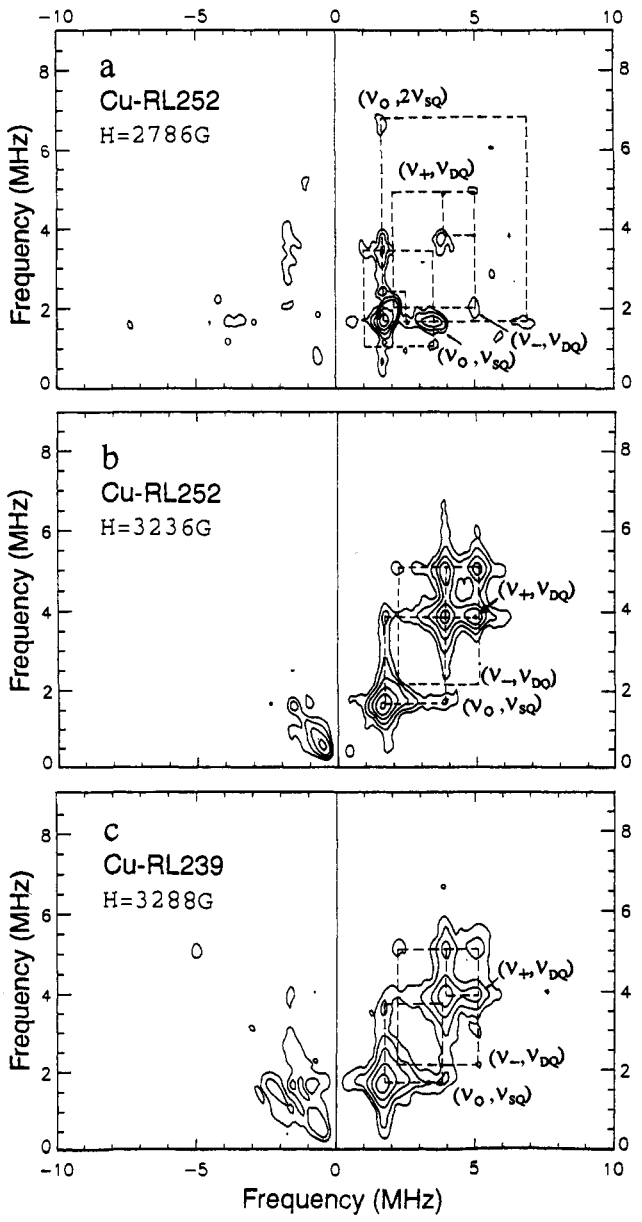

Figure 6. 2D HYSCORE spectra (contour plots) of (a) Cu−RL252 in CH_3CN recorded at 5 K, $\tau = 0.35$ μs, $\nu = 9.32$ GHz, $H_o = 2786$ G; (b) same but $H_o = 3236$ G (max echo position). (c) Cu−RL239 in CH_3CN recorded at 12 K, $\tau = 0.3$ μs, $\nu = 9.47$ GHz, $H_o = 3288$ G (max echo position).

Table 2. The ESEEM Frequencies Observed for Cu−RL252 and Cu−RL239 and Their Assignments

Cu−RL252 (MHz)	Cu−RL239 (MHz)	assignment	comment
1.66−1.71	1.71−1.8	ν_o	
2.15	2.2	ν_-	
3.3	3.32	ν_{SQ}	
3.5−3.8	3.46	ν_{SQ_1}	only at $\sim g_{\|\|}$
1.4−1.5	1.27	ν_{SQ_2}	only at $\sim g_{\|\|}$
3.86−3.91	3.96	ν_+	
5.0	5.1−5.2	ν_{DQ}	
5.5		$\nu_o + \nu_+$	
7.4	7.7	$2\nu_{SQ}$	

contributing to the echo increases significantly and only the ν_+ component of the peak is detected. The field dependence of ν_{SQ_1} is well illustrated by following its sum combination signal, $2\nu_{SQ_1}$, at 7−8 MHz (see Figures 4a and 5a). To summarize, Table 2 lists all the observed peaks and their assignments. From the frequencies and eqs 4 and 5, we estimate $e^2qQ/h \cong$ 4.04 MHz, $\eta \cong 0.85$, and $a_{iso} \approx 1.2$−1.5 MHz for the hydroxamate nitrogens in Cu−RL252.

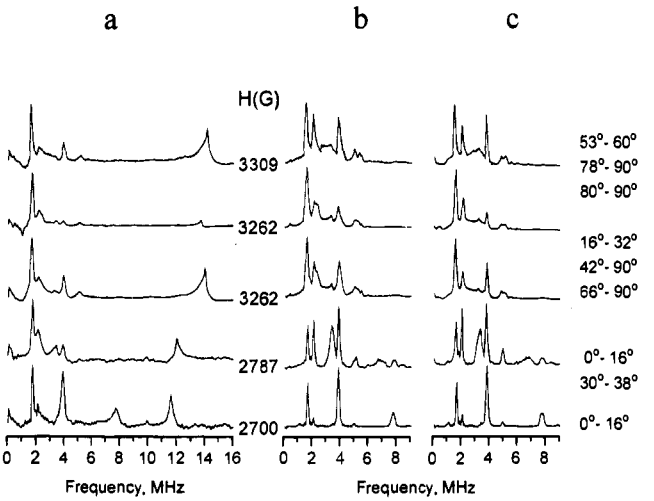

Figure 7. (a) Experimental three-pulse FT-ESEEM spectra of Cu−RL239 in MeOH recorded at 12 K and $\tau = 0.3$ μs. The spectrum recorded at 3262 G was obtained with $\tau = 0.22$ μs. The spectrum recorded at 2787 G was obtained at 9.26 GHz whereas all the other at 9.47 GHz. (b, c) Simulated spectra obtained with parameter sets A and B for Cu−RL239, respectively, as listed in Table 3. The angles listed on the right side correspond to the range of θ_o used in the simulations.

The 1D ESEEM spectra of Cu−RL239 are very similar to those of Cu−RL252. This is not surprising because the EPR spectra are not indicative of a radically different structure. Orientation−selective three-pulse FT-ESEEM spectra of Cu−RL239 in methanol are shown in Figure 7a. The ν_o, ν_-, and ν_+ peaks appear at 1.71−1.8, 2.2, and 3.9 MHz, respectively, and ν_{DQ} is found at 5.1−5.2 MHz. From these values, $e^2qQ/h \cong 4.1$ MHz, $\eta \cong 0.83$, and $a_{iso} \cong 1.5$ MHz are calculated. These values are only slightly different from those of Cu−RL252. As in Cu−RL252, the spectrum recorded close to the $g_{||}$ edge of $M_I(Cu) = -3/2$ shows a strong peak at 3.9 MHz, assigned to ν_{SQ_1}. In all spectra, the intensity of the ν_+ peak is somewhat reduced in comparison to the spectra of Cu−RL252 (see Figure 4a). The 2D HYSCORE spectrum of Cu−RL239 recorded at 3288 G ($g = 2.058$) and $\tau = 0.3$ μs (Figure 6c) confirms the assignment of the 5.1 MHz peak to ν_{DQ} and of the peak at 3.9 MHz to a superposition of ν_+ and ν_{SQ_1} based on the cross peak at (5.1 MHz, ν_+) and the ridge at (2−3.9 MHz, ν_o).

Simulations. In order to determine the anisotropic part of the hyperfine interaction and the orientation of the principal axis systems of the quadrupole and hyperfine interactions with respect to the principal axis system of **g**, computer simulations of the orientation-selective 1D ESEEM spectra were performed. The simulations were carried out for two chemically equivalent nitrogens related either by C_2 (*trans*) or σ_{xz} (*cis*) symmetry (see Figure 2).[9] Three-pulse FT-ESEEM spectra calculated for the two structures showed no significant differences.

The appearance of a rather narrow ν_{SQ_1} peak when the field is set to $g_{||}$ ($M_I(Cu) = -3/2$) indicates that at this orientation the inhomogeneous broadening due to the quadrupole interaction is minimal. Although a minimum range of the complex orientations (θ_o) is excited when the magnetic field is set to this position, a disorder with respect to the ^{14}N hyperfine and quadrupole interactions is still possible, depending on the relative orientation of the principal axis system of these tensors and that of the g matrix. While the range of θ_o is small, a full integration over ϕ_o is still required, and the latter is the source of possible disorder. When $\eta \approx 1$, minimum disorder is achieved when either the y'' or z'' principal axes of the quadrupole tensor are approximately parallel to the $g_{||}$ direction, thus $\beta \approx 0°$ or 90°.

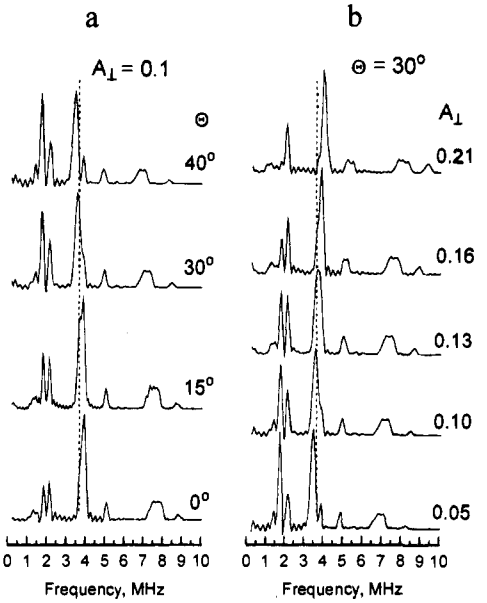

Figure 8. Simulated three-pulse FT-ESEEM spectra calculated with $H_o = 2400$ G, $\nu = 8.46$ GHz, $\tau = 0.22$ μs, $\theta_o = 0-24°$ and $\beta = \gamma = \phi = 0°$. (a) The dependence on θ for $A_\perp = 0.1$ MHz. The values of e^2qQ/h, η, and A_{iso} were, from top to bottom, 3.99 MHz, 0.815, 0.82 MHz; 3.98 MHz, 0.835, 0.74 MHz; 3.98 MHz, 0.85, 0.70 MHz; 3.98 MHz, 0.85, 0.68 MHz; 3.99 MHz, 0.85, 0.68 MHz. (b) The dependence on $A_\perp$ for $\theta = 30°$. The values for e^2qQ/h, η, and A_{iso} were, from top to bottom, 4 MHz, 0.85, 0.66 MHz; 3.98 MHz, 0.85, 0.68 MHz; 4 MHz, 0.845, 0.72 MHz; 4 MHz, 0.845, 0.74 MHz.

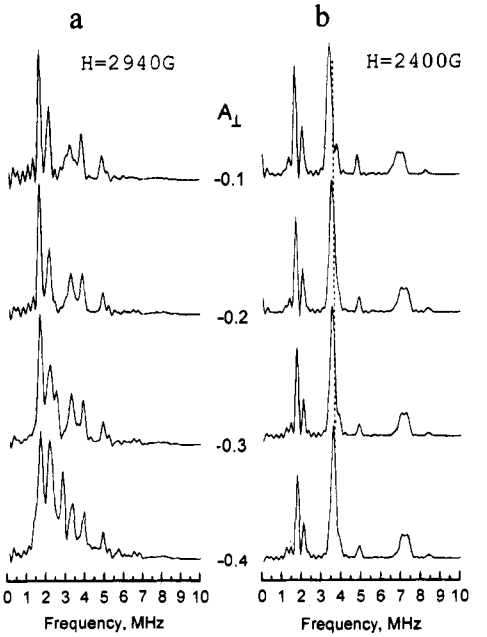

Figure 9. Simulated three-pulse FT-ESEEM spectra calculated for $\beta = \alpha = \theta = 90°$; $\gamma = \phi = 90°$ and $\tau = 0.22$ μs as a function of $A_\perp$ for (a) $H_o = 2940$ G; (b) $H_o = 2400$ G. The values of e^2qQ/h, η, and A_{iso} were, from top to bottom, 4.0 MHz, 0.86, 0.67 MHz; 4.0 MHz, 0.86, 0.61 MHz; 4.0 MHz, 0.88, 0.649 MHz; 4.0 MHz, 0.88, 0.40 MHz.

These orientations and the estimated values of e^2qQ/h, η, and a_{iso} obtained from the peaks positions were used as a starting point in the simulation procedure where we searched for values of α, θ, and $A_\perp$ and refined the above parameters to reproduce the experimental positions and relative intensities of all peaks. This was done separately for the two cases of $\beta = 0°$ and 90°.

While many sets of parameters could reproduce the spectrum at the $g_\perp$ region, simulating ν_{SQ_I} at the $g_{||}(M_I(Cu) = -3/2)$ region was more difficult. Among the well-resolved lines in these spectra ν_{SQ_I} was found to be most sensitive to θ, $A_\perp$, and A_{iso}, and it was therefore used as the main feature for the determination of θ and $A_\perp$ and the refinement of A_{iso}. For $\beta = 0°$, the position of ν_{SQ_I} could be reproduced with small values of θ, $A_{iso} > 0$, and $A_\perp > 0$ (or, alternatively, with $A_{iso} < 0$ and $A_\perp < 0$). This is shown in Figure 8a, where simulated spectra, calculated for the low field edge and $A_\perp = 0.1$ MHz, are depicted as a function of θ. In Figure 8b, θ is kept constant at 30° and $A_\perp$ is varied. Rather than keeping the parameters e^2qQ/h, η, and A_{iso} constant they were slightly refined for each spectrum in order to reproduce the NQR and ν_{DQ} frequencies and show how θ and $A_\perp$ were determined from the simulations. The dependence of the ~7.3 MHz signal on A_{iso} indicates that it is due to sum combination of ν_{SQ_I} rather than of ν_+. This also explains why this peak is observed in the experimental spectra only at low fields (see Figures 4a and 5a) where the intensity of ν_{SQ_I} is large. Comparison of the experimental spectra (Figure 4a) and the calculated spectra of Figure 8 shows that the best agreement is achieved for $\theta \approx 15°$. Nevertheless spectra calculated with these parameters for fields within the center of the EPR powder pattern ($H_o = 2900$ G) exhibit a too intense ν_- peak for $\tau = 0.3$ μs.

The frequency and intensity of ν_{SQ_I} can be reproduced also with $A_{iso} > 0$, $A_\perp < 0$, and $\theta = 90°$. Figure 9 shows examples of simulated spectra for $A_\perp = -(0.1 - 0.4)$ MHz, calculated for the low field $g_{||}$ edge and for the $g_\perp$ position. The best agreement for both fields is achieved when $A_\perp = -0.2$ MHz. The same spectra were obtained for $A_{iso} < 0$ and $A_\perp > 0$. In general, the spectra were not very sensitive to φ and γ, and they were therefore arbitrarily set to 0. The simulated spectra shown in Figures 8 and 9 were calculated for $\nu = 8.46$ GHz which is lower than the frequency at which the experimental spectra shown in Figures 4 and 5 were measured ($\nu = 9.15$ GHz). The trends observed, however, are similar at both frequencies.

Spectra calculated for the low field edge with $\alpha = \theta = \beta = 90°$ also exhibit a ν_{SQ_I} peak at 3.71 MHz for $A_\perp = -(0.1-0.2)$ MHz. The relative intensities of the ν_o and ν_- peaks, however, are not satisfactory. Moreover, spectra calculated with the same parameters for the $g_\perp$ position did not reproduce the experimental spectra well, the major problem being the intensity and line shape of ν_o and ν_- peaks. The case of $\beta = 90°$ and $\alpha = 0°$ was excluded since the sum combination harmonic of ν_{SQ_I} at 7.3 MHz could not be reproduced, indicating that the signal appearing at 3.8 MHz is ν_+ and not ν_{SQ_I}. We failed to find any other sets of parameters and values of β between 0–90° that reproduced the experimental spectra satisfactorily.

Finally, two best fit sets of parameters, listed in Table 3, were found. The quadrupole tensor parameters in both sets are similar, but the sets differ in $A_\perp$ and θ. Note that both sets yield very similar values for the hyperfine couplings along $g_{||}$. Using these parameters, all orientation-selective three-pulse FT-ESEEM spectra in Figures 4a and 5a were simulated (Figures 4c,d and 5c,d). Both sets exhibit a good agreement with the experimental spectra, and we cannot prefer one set over the other only on the basis of their agreement with the experimental data. This demonstrates the limitations of the orientation selective experiment, where only at one field position a single crystal-like spectrum is observed. Comparison of simulated spectra with the best fit parameters for one and two ^{14}N nuclei show that while the peak at 7.3 MHz (observed at $H_o = 2648-2700$ G) is a sum combination of ν_{SQ_I}, the signal at 3.27 MHz ($H = 2900-3300$ G) is not a sum combination of ν_o but rather corresponds to a singularity of one of the single quantum powder patterns.

The orientation-selective ESEEM spectra of Cu–RL239 could also be simulated satisfactorily with two sets of Hamil-

Table 3. Best-Fit Spin Hamiltonian Parameters (Used in Figures 4, 5, and 7) As Determined from the Simulations of the Orientation-Selective Three-Pulse ESEEM Spectra

	set	$\lvert e^2qQ/h\rvert$ (MHz ± 0.02)	$\eta \pm 0.01$	α, β, γ (deg ± 10)	a_{iso} (MHz ± 0.1[a])	$A_\perp$ (MHz ± 0.05[a])	$a_\perp$ (MHz ± 0.1[a])	θ (deg ± 10)	ϕ (deg ± 10)
Cu−RL252	A	3.9	0.85	0	±1.28	∓0.2	∓0.43	90	0
Cu−RL252	B	3.9	0.85	0	±1.28	∓0.1	∓0.21	15	0
Cu−RL239	A	4.0	0.86	0	±1.25	∓0.26	∓0.55	90	0
Cu−RL239	B	4.01	0.86	0	±1.36	±0.12	±0.26	15	0

[a] The relatively small uncertainty is due to the high sensitivity of ν_{SQ} to the hyperfine parameters.

tonian parameters, differing from each other mainly in the amplitude and orientation of the hyperfine interaction as listed in Table 3. The simulated spectra are presented in Figure 7b,c. As for Cu−RL252, the two options could not be distinguished. The best fit sets of parameters for Cu−RL239 and Cu−RL252 are very similar; the major differences are the slightly larger quadrupole coupling constant and anisotropic hyperfine component in Cu−RL239. This is manifested mainly in the subtle shifts of ν_o and ν_{DQ} and the apparent broadening of ν_-, which is probably a consequence of overlap with a ν_{SQ} signal.

In order to differentiate between *cis* and *trans* configurations of the complexes we compared the modulation depth of the ESEEM waveforms calculated with the best fit parameters relating the parameters of the two nitrogens according to the symmetry of the binding site.[9] Unfortunately, the differences observed were not significant enough to draw unambiguous conclusions regarding the configuration. We note, however, that in the case of Cu−RL239 a *trans* configuration is very unlikely due to steric constraints.

Discussion

Ab-initio SCF-MO calculations, performed by Ruiqin *et al.*[31] on several substituted hydroxamic acids, and previous ESEEM results on VO−RL261[9] (see Figure 1) show that the principal axis of the ^{14}N quadrupole tensor, z'', is along the nitrogen lone pair, perpendicular to the C−N−O plane. Therefore, $\beta = 0°$ indicates that the hydroxamate planes are perpendicular to the $g_{||}$ direction, which is to a good approximation along the symmetry axis of the complex, as found for Cu(II) acetyl acetonate (acac).[32] Hence, the complex has either a square coplanar structure or an octahedral structure with an elongated tetragonal distortion. Comparison of the best fit parameters obtained for the Cu(II) and the VO(II) bis-hydroxamate (Q = 3.8, 4.0 MHz; η = 0.84, 0.91, respectively) shows that the quadrupole coupling constant and the asymmetry parameters are very similar. This implies that the quadrupole coupling constant is relatively invariant to the type of ion bound. Nevertheless, the quadrupole coupling constant in the complexes is significantly reduced compared to that of substituted hydroxamic acids (4.6−5.2 MHz).[31] The reduction in the quadrupole coupling constant is attributed to some delocalization of the nitrogen lone pair over the O−C−N−O structure.[9]

The comparison between similar Cu(II) and VO(II) complexes is of interest due to their complementary configurations, d^9 *vs* d^1. Superhyperfine ligand couplings are usually larger in Cu(II) complexes than in VO(II) complexes. For example, while the isotropic hyperfine constant of directly bound nitrogens is usually in the range of 6−7 MHz for VO(II),[33−37] it is 30−40 MHz for Cu(II).[32,36,38−40] The large difference stems from their different electronic structures. In Cu(II), in a tetragonal symmetry, which is ubiquitous for Cu(II), the unpaired electron resides in the b_{1g} molecular orbital, the lobes of which are directed toward the ligands as it contains contributions from both the copper $d_{x^2-y^2}$ orbital and the σ orbitals of the ligands.[32] The mixing of the ligand's σ orbitals leads to a significant superhyperfine interaction. For vanadyl in a C_{4v} symmetry the unpaired electron resides in a b_{2g} orbital which is a linear combination of the vanadium d_{xy} orbital and in-plane p orbitals of the ligands.[41] The lobes of this molecular orbital are pointing between the ligands, and therefore, the nitrogen hyperfine is mostly a consequence of mixing in the π plane which is usually small. Hence, in VO(II) the unpaired electron is almost completely localized on the vanadium d_{xy} orbital, and the ligand hyperfine couplings are small.[37] The comparable values of ^{14}N hyperfine interactions in the copper and vanadyl bis-hydroxamate complexes are thus unexpected. In the VO(II) complexes a_{iso} = 1.8 MHz and $a_\perp$ = 0.6−0.7 MHz,[9] and in the Cu(II) complexes the values are somewhat lower, $a_{iso} \cong$ 1.3 MHz and $a_\perp$ = 0.2−0.6 MHz.

Comparison of the tetra-imidazole complexes of Cu(II) and VO(II) shows that the hyperfine coupling of both the directly bound nitrogen and the remote nitrogens are significantly larger in the Cu(II) complex (39.4[42] and 1.75[43] MHz, respectively) than in the VO(II) complexes (6−7[33] and 0.3[44] MHz, respectively). The isotropic hyperfine constant of the remote nitrogen, which is three bonds away from the metal ion, is comparable to that of the nitrogen in Cu(II) bis(*N*,*N*-di-*n*-butyldithiocarbamate), a_{iso} = 1.25 MHz, which is also three bonds away from Cu(II).[45] In this complex, a_{iso} of the directly bound ^{33}S is 34.8 MHz,[45] which corresponds to a value of 32.7 MHz for ^{14}N, considering only the different gyromagnetic ratios. This value is in the order of those found in imidazole complexes.

The bis-hydroxamate binders, which are bidentate chelates, consist of two hydroxamate groups each, and the donors are the two oxygens (see Figure 1). Therefore, the ground state of the Cu(II) complexes should also be mostly of a d_{xy} character

(31) Ruiqin, W.; Xiaolan, Y.; Zhenye, F.; Haq, M. M. I.; Khurshid, M. M. P.; Payner, T. J.; Smith, A. S.; Palmer, M. H. *J. Am. Chem. Soc.* **1989**, *111*, 114.
(32) Maki, A. S.; McGarvey, B. R. *J. Chem. Phys.* **1958**, *29*, 31.
(33) Dikanov, S. A.; Tyryshkin, A. M.; Hüttermann, J.; Bogumil, R.; Witzel, H. *J. Am. Chem. Soc.* **1995**, *117*, 4976, Table 2 and reference therein.
(34) Reijerse, E. J.; Shane, J. J.; de Boer, E.; Collison, D. In *Electron Magnetic Resonance of Disordered Systems*; Yordanov, N. D., Ed.; World Scientific: Singapore, 1989; p 189.
(35) Astashkin, A. V.; Dikanov, S. A.; Tsvetkov, Yu. D. *J. Struct. Chem.* **1985**, *26*, 363.
(36) Goslar, J.; Piekara-Sady, L.; Kispert, L. In *Handbook of Electron Spin Resonance*; Poole, C. P., Jr., Farach, H. F., Eds.; AIP Press: New York, 1994; p 360.
(37) Kivelson, D.; Lee, S.-K. *J. Chem. Phys.* **1964**, *41*, 1896.
(38) Werst, M. M.; Davoust, C. E.; Hoffman, B. M. *J. Am. Chem. Soc.* **1991**, *113*, 1533.
(39) Harrison, S. E.; Assour, J. M. *J. Chem. Phys.* **1965**, *43*, 1746.
(40) Kivelson, D.; Neiman, R. *J. Chem. Phys.* **1961**, *35*, 149.
(41) Ballhausen, C. J.; Gray, H. B. *Inorg. Chem.* **1962**, *1*, 111.
(42) Sholl, H.-J.; Hüttermann, J. *J. Phys. Chem.* **1992**, *96*, 9684.
(43) Mondovi, B.; Graziani, M. T.; Mims, W. B.; Oltzik, R.; Peisach, J. *Biochemistry* **1977**, *16*, 4198. McCracken, J.; Pember, S.; Benkovic, S. J.; Villafranca, J. J.; Miller, R. J.; Peisach, J. *J. Am. Chem. Soc.* **1988**, *110*, 1069. McCracken, J.; Peisach, J.; Dooley, D. M. *J. Am. Chem. Soc.* **1987**, *109*, 4064.
(44) Dikanov, S. A.; Burgard, C.; Huttermann, J. *Chem. Phys. Lett.* **1993**, *212*, 493.
(45) Reijerse, E. J.; Paulissen, M. L. H.; Keijzers, C. P. *J. Magn. Reson.* **1984**, *60*, 66.

as in $Cu(acac)_2$[46-48] and in Cu(II) bis-dithiocarbamate.[49] EPR single crystal studies of Cu(II) ketoenolato complexes showed that the g_{xx} and g_{yy} directions, where the x and y axes were defined along the directions of the out of plane π orbitals d_{xz} and d_{yz}, are in between the oxygen ligands, in the nodes of the ground state orbital.[46] Hence, the unpaired electron resides in a molecular orbital with a d_{xy} character, the lobes of which are directed mostly toward the ligands,[46] similar to many cases where the ground state has a $d_{x^2-y^2}$ character. It is therefore expected that also in the bis-hydroxamate copper complexes, as in the imidazoles and thiocarbamates, there will be a significant spin density on the directly bound nuclei (oxygens) due to mixing with σ orbitals. The relatively small couplings found for the nitrogen, which is similar to that found on nitrogens three bonds away and to that of the VO(II) complex, may thus indicate that the ground state molecular orbital has a node at the nitrogen. Whether this behavior is unique to the hydroxamate binders or represents a general trend in Cu(II) coordination to chelates is an open question due to the lack of more experimental examples and detailed MO calculations. We note, however, that a similar situation has been observed in Cu(II) bis(*cis*-1,2-dicyanoethylenedithiolate), where the hyperfine couplings of the $^{13}C_{1,2}$ situated two bonds away from the Cu(II) (a_{iso} = −4.0, −3.81 MHz) are smaller than those of the $^{13}C_{3,4}$ which are three bonds away (a_{iso} = 5.83, 5.56 MHz).[50] In this case, extended Hückel molecular orbital calculations were performed, showing that the coefficients of the atomic orbitals of $C_{1,2}$ in the wave function of the unpaired electron are smaller than those of $C_{3,4}$. Using the values obtained for $^{13}C_{1,2}$, a rough estimate of ≃1 MHz is obtained for a ^{14}N two bonds away. This is the order of the values found in Cu−RL252 and Cu−RL239. One, however, has to remember that the comparison with the dithiolene complex is rather coarse since our system involves negatively charged oxygen donors rather than neutral sulfurs.

The ^{14}N isotropic hyperfine coupling of the VO(II) complexes, 1.8 MHz, is between the values obtained for directly bound nitrogen and nitrogen situated three bonds away. This value is comparable to other hyperfine couplings with nuclei situated 2 bonds away from the vanadium in VO(II) complexes such as values of 5.4 and 5.0 MHz for ^{13}C in $VO(glicinate)_2$ and $VO([2\text{-}^{13}C]pyruvate)_2$.[51] These values scale down to 1.54 and 1.42 MHz for ^{14}N.

For both Cu−RL252 and Cu−RL239, the simulations generated two possible sets of parameters for the hyperfine interaction (see Table 3). In the first set (A), the principal axis z' is approximately perpendicular to the O−C−N−O plane ($\theta \sim 15°$), whereas in the second set (B), it is in the plane ($\theta \sim 90°$). Set A implies that the major contribution to the anisotropic hyperfine interaction comes from spin density in the p_π orbital of the nitrogen. The mechanism leading to a finite spin density in the nitrogen p_π orbital could be exchange polarization from the d_{xy} orbital to the d_{xz} and/or d_{yz} orbitals involved in the π bonding. In this case, however, the anisotropic hyperfine interaction should not have axial symmetry as was initially assumed. The second option suggests that the anisotropic hyperfine interaction is dominated mainly by the dipole−dipole interaction between the unpaired electron on the metal ion and the nitrogen. The value of $|a_\perp|$ = 0.43 MHz corresponds to a Cu−N distance of 2.35 Å. Rough calculations of the Cu−N distance taking the Cu−O distance as 2 Å, the N−O bond as 1.4 Å, and a Cu−O−N angle of 120° yields a Cu−N distance around 2.8 Å. This is significantly larger than the experimental value and indicates that the point−dipole approximation is not valid and that there are additional contributions to the anisotropic hyperfine coupling. This is not surprising as in Cu(II) complexes with substituted imidazole $a_\perp$ of the remote nitrogen was found to depend on the substituent.[52]

Finally, the differences found between the Cu−RL239 and Cu−RL252 systems are small, manifested mainly in the magnitude of $a_\perp$, which for both sets A and B was larger in Cu−RL239. Interestingly, $a_\perp$ is also larger in VO−RL239 than in VO−RL261.[9] While both RL252 and RL261 contain amino acid bridges, alanine and leucine, respectively, this bridge is absent in RL239. The different properties of the amide and the $O-CH_2$ groups apparently affect the electron distribution in the binding sites, leading to small changes in $a_\perp$. Inspection of molecular models suggests that the square planar Cu(II) complex of RL239 is only feasible in a cisoid, rather than a transoid arrangement. The remarkably sharp signals of Cu−RL252 are suggestive of a highly defined complex that adopts a single conformation. Whether the preferred configuration for the more flexible Cu−RL252 complex is cisoid or transoid is not possible to determine from the experimental results.

Conclusions

The hyperfine coupling of the nitrogens in the hydroxamate groups falls within the "cancellation condition" range at 8−9 GHz leading to an exceptionally well-resolved ESEEM spectrum consisting of the NQR frequencies, ν_{DQ} and ν_{SQ}. The latter is rarely detected in orientationally disordered systems. Complete assignment of all signals in the orientation-selective ESEEM spectra was achieved using 2D HYSCORE experiments. Computer simulations of the orientation-selective 1D ESEEM spectra gave the ^{14}N hyperfine and quadrupolar parameters which indicated that the structure of the binding site of both Cu−RL252 and the parent Cu−RL239 is close square coplanar. The appearance of ν_{SQ} provided excellent constraints on the simulations, leading to a more accurate determination of the Hamiltonian parameters. The relatively small ^{14}N hyperfine coupling, found for both complexes, is attributed to a node in the molecular orbital, occupied by the unpaired electron, at the nitrogen. Only minor differences in the Hamiltonian parameters of Cu−RL252 and Cu−RL239 were detected, the quadrupole parameters and the anisotropic hyperfine component being slightly larger in Cu−RL239. These subtle differences indicate that the amido bridge practically does not affect the binding site geometry.

Acknowledgments. This research was supported by the Israel Science Foundation administered by the Israel Academy of Sciences and Humanities and partially by the US−Israel Binational Science Foundation (Grant 90-00128). We thank Dr. Ed. Reijerse from the University of Nijmegen for performing C-band (4−5 GHz) ESEEM measurements and Dr. D. van Ormondt for giving us the LPSVD computer program. S.A.D. thanks the Department of Chemical Physics at the Weizmann Institute of Science for supporting his stay at this Institute and for the hospitality shown. Part of this work was also sponsored by the U.S. Department of Energy under contract DE-AC06-76 RLO and by Associated Western Universities, Inc., Northwest Division, under Grant DE-FG06-89 ER-75522 or DE-FG06-92RI-12451 with the U.S. Department of Energy.

JA9519795

(46) Hitchman, M. A.; Olson, C. D.; Belford, R. L. *J. Chem. Phys.* **1969**, *50*, 1195.
(47) Funck, L. L.; Ortolano, T. R. *Inorg. Chem.* **1968**, *7*, 507.
(48) Hathaway, B. J.; Billing, D. E. *Coord. Chem. Rev.* **1970**, *5*, 143.
(49) Keijzers, C. P.; Smaathrorst. *Chem. Phys. Lett.* **1980**, *69*, 2.
(50) Kirmse, R.; Stach, J.; Abram, U.; Dietzch, W.; Böttcher, R.; Gribnau, M. C. M.; Keijzers, C. P. *Inorg. Chem.* **1984**, *23*, 3333.
(51) Tipton, P. A.; McCracken, J.; Cornelius, J. B.; Peisach, J. *Biochemistry* **1988**, *28*, 5720.
(52) Jiang, F.; McCracken, J.; Peisach, J. *J. Am. Chem. Soc.* **1990**, *112*, 9035.